Disentangling the effect of regional SST bias on the double-ITCZ problem

Jiheun Lee, Sarah M. Kang* and Hanjun Kim

Department of Urban and Environmental Engineering, Ulsan National Institute of Science and Technology, Ulsan, Republic of Korea

Baoqiang Xiang

NOAA/Geophysical Fluid Dynamics Laboratory, Princeton, New Jersey, USA

University Corporation for Atmospheric Research, Boulder, Colorado, USA

*Corresponding author: Sarah M. Kang, Department of Urban and Environmental Engineering, Ulsan National Institute of Science and Technology, UNIST-gil 50, Ulsan 689-798, Republic of Korea. E-mail: skang@unist.ac.kr

Abstract

This study investigates the causes of the double intertropical convergence zone (ITCZ) bias, characterized by too northward northern Pacific ITCZ, too dry equatorial Pacific, and too zonally elongated southern Pacific rainband. While the biases within one fully coupled model GFDL CM2.1 are examined, the large-scale bias patterns are broadly common to CMIP5/6 models. We disentangle the individual contribution of regional sea surface temperature (SST) biases to the double-ITCZ bias pattern using a series of slab ocean model experiments. A previously suggested Southern Ocean warm bias effect in displacing the zonal-mean ITCZ southward is manifested in the northern Pacific ITCZ while having little contribution to the zonally elongated wet bias south of the equatorial Pacific. The excessive southern Pacific precipitation is instead induced by the warm bias along the west coast of South America. The Southern Ocean bias effect on the zonal-mean ITCZ position is diminished by the neighboring midlatitude bias of opposite sign in GFDL CM2.1. As a result, the northern extratropical cold bias turns out to be most responsible for a southward-displaced zonal-mean ITCZ. However, this southward ITCZ displacement results from the northern Pacific branch, so ironically fixing the extratropical biases only deteriorates the northern Pacific precipitation bias. Thus, we emphasize that the zonal-mean diagnostics poorly represent the spatial pattern of the tropical Pacific response. Examination of longitude-latitude structure indicates that the overall tropical precipitation bias is mostly locally driven from the tropical SST bias. While our model experiments are idealized with no ocean dynamics, the results shed light on where preferential foci should be applied in model development to improve particular features of tropical precipitation bias.

Keywords

Tropical precipitation bias, Double-ITCZ problem, Regional SST biases, Atmospheric energy transport

Acknowledgements

This work was supported by the National Research Foundation of Korea (NRF) grant (NRF-2020R1A2C210150311) funded by the Ministry of Science and ICT (MSIT) of South Korea. The authors are grateful to Hideaki Kawai and the two anonymous reviewers for their constructive comments that greatly improved the manuscript.

Declarations

Funding

This work was supported by the National Research Foundation of Korea (NRF) grant (NRF-2020R1A2C210150311) funded by the Ministry of Science and ICT (MSIT) of South Korea.

Conflicts of interest

The authors declare no competing interests.

Availability of data and material

The output from CMIP5 and CMIP6 are provided by the World Climate Research Programme's Working Group on Coupled Modelling and are available at https://esgf-node.llnl.gov/projects/cmip5 and https://esgf-node.llnl.gov/search/cmip6. Model and observational data used in this paper's analysis is permanently accessible in Zenodo with the identifier https://doi.org/10.5281/zenodo.5062468.

Code availability

Not applicable

Author's contributions

Not applicable

Ethics approval

Not applicable

Consent to participate

Not applicable

Consent for publication

Not applicable

1. Introduction

Climate models' fidelity in projecting the future climate relies on their ability to accurately simulate the mean climate state (Shukla et al. 2006). Since the early days of model development, most climate models had difficulty reproducing precipitation distributions at regional scales, thus impairing the fidelity of their future projections. One of the most pervasive and persistent model biases, known as the double-intertropical convergence zone (ITCZ) phenomenon, involves a complex spatial structure in the tropics, and thus likely reflects multiple regional biases.

In the zonal-mean perspective, the precipitation bias can be decomposed into the hemispherically symmetric and anti-symmetric components (Adam et al. 2016; Kim et al. 2021). The symmetric component is characterized by excessive precipitation off the equator and deficient equatorial precipitation (Lin 2007), linked to the biases in net energy input (NEI) to the atmospheric column in the equatorial region (Adam et al. 2016; Bischoff and Schneider 2016), particularly owing to the erroneous ocean heat uptake associated with the equatorial upwelling (Kim et al. 2021). By contrast, the anti-symmetric component displays a precipitation deficit to the north and an excess to the south of the equator (Li and Xie 2014), linked to the hemispherically asymmetric biases in the atmospheric column energy via the so-called energetics framework (e.g., Kang et al. 2008). The hemispheric asymmetry of top-of-atmosphere radiation bias in the extratropics is pointed out to be the cause of the hemispherically anti-symmetric component of tropical precipitation bias (Adam et al. 2016). In particular, too much energy flux into the atmosphere over the Southern Ocean associated with cloud biases is suggested to cause anomalously northward atmospheric energy transport across the equator, leading to excessive precipitation in the southern relative to the northern tropics (Hwang and Frierson 2013). While some fully coupled model studies indicate that the

107 radiation bias correction over the Southern Ocean leads to only a limited improvement of the
108 double-ITCZ bias owing to the compensating effect of a dynamic ocean (Hawcroft et al. 2017;
109 Kay et al. 2016; Xiang et al. 2018), other fully coupled model studies report a significantly
110 alleviated double-ITCZ bias through the improvement in the Southern Ocean radiation bias
111 (Mechoso et al. 2016; Kawai et al. 2021). A multi-model study shows that radiative cooling
112 over the Southern Ocean robustly shifts the tropical precipitation northward, albeit with a
113 substantial model spread (Kang et al. 2019). With regard to an intermodel uncertainty, the
114 hemispherically anti-symmetric component of double-ITCZ bias is tied to the tropical
115 asymmetry in net surface heat flux estimated from their corresponding Atmospheric Model
116 Intercomparison Project (AMIP) simulations (Xiang et al. 2017).

117 The zonal-mean characteristics of tropical precipitation bias average out the rich regional
118 structures (e.g., Figure 1c). We first examine the regional variations embedded in the
119 hemispherically symmetric component. The dry zonal-mean bias on the equator is mostly
120 concentrated in the Pacific basin, accompanied by an excessive cold tongue bias that extends
121 too far west due to overly strong trade winds (Lin 2007; De Szoeke and Xie 2008). Too strong
122 trade winds are recently attributed to the underestimated blocking effect of the low biased
123 Central American orography on the prevailing easterlies into the northeastern tropical Pacific
124 (Baldwin et al. 2021). Meanwhile, the wet zonal-mean bias straddling the equator comprises
125 the northward-shifted northern Pacific ITCZ and too zonally elongated southern tropical
126 Pacific rainband. The excessive southeastern Pacific precipitation (Oueslati and Bellon 2015)
127 has been linked with a number of factors, including the model-dependent SST threshold
128 required for the onset of deep convection (Bellucci et al. 2010), warm sea surface temperature
129 (SST) biases associated with the underestimated stratus cloud fraction off the coast of Peru (Ma
130 et al. 1996), the smoothing of the Andes orography in climate models (Takahashi and Battisti

131 2007), and weaker-than-observed alongshore winds (Zheng et al. 2011). Improved simulation
132 of low-level cloud fractions alleviates the SST and rainfall biases in the SEP but exacerbates
133 the equatorial dry and cold tongue biases (Fushan et al. 2005), implying a limited improvement
134 of the overall double-ITCZ bias. This hemispherically symmetric component dominates the
135 intermodel uncertainty in the zonally averaged tropical precipitation pattern (Kim et al. 2021).
136 By contrast, the hemispherically asymmetric component, characterized by the southward-
137 biased zonal-mean ITCZ, is a result of the overall wet bias in the southern tropical Pacific as
138 well as a relatively small net bias in the northern tropics due to the dipole structure of the
139 northern Pacific associated with the northward-biased northern ITCZ.

140 Despite the rich spatial structure of the double-ITCZ bias, previous studies often targeted
141 one single feature, so that the overall bias correction has been limited because improvement in
142 one feature may lead to deterioration of another. As a result, the double-ITCZ problem has
143 been persistent over three Coupled Model Intercomparison Project (CMIP) phases (Mechoso
144 et al. 1995; De Szoeke and Xie 2008; Zhang et al. 2015; Tian and Dong 2020). The double-
145 ITCZ bias imposes a significant barrier to the simulation of the leading mode of tropical Pacific
146 variability, El Niño–Southern Oscillation (Guilyardi et al. 2003; Ham and Kug 2014), and also
147 to model projections of the Pacific warming pattern under greenhouse gas increases (Zhou and
148 Xie 2015; Seager et al. 2019). The double-ITCZ bias is also related to the equilibrium climate
149 sensitivity, the global mean surface air temperature increase following a CO_2 doubling, which
150 is a measure of the severity of global climate change (Tian 2015).

151 Identifying the bias sources is a necessary step for improving the simulations of the tropical
152 precipitation distribution. In this study, we systematically design model experiments to identify
153 the contribution of regional SST biases to the specific characteristics of tropical precipitation
154 biases. We use “regional” to refer to the different latitude bands as well as the departure from

155 the zonal mean. Tropical precipitation is closely linked to SSTs (Lindzen and Nigam 1987),
156 which are determined by both local and remote processes. To take into account the impact of
157 the SST biases outside the tropics on the tropical precipitation distribution, we adopt an
158 atmosphere-slab ocean climate model with a prescribed q-flux that replicates the SST bias
159 instead of directly manipulating the SSTs (Kang and Held 2012). The surface energy budget is
160 closed in the slab ocean whereas it is not constrained with fixed SSTs. Hence, the slab ocean
161 configuration instead of the AMIP-type simulation with prescribed SSTs permits us to evaluate
162 the role of energetic constraints in forming the double-ITCZ. Our experiment setting offers a
163 unified perspective for interpreting the overall double-ITCZ bias by allowing us to assess the
164 manifestation of regional SST biases in the spatial pattern of tropical precipitation. More details
165 of the experiment set-up are offered in section 2. We then provide some insights into the
166 relative roles played by tropical versus extratropical SST biases in developing the double-ITCZ
167 in section 3.1. The tropical bias is decomposed into the zonally symmetric and asymmetric
168 components in section 3.2. The extratropical bias is separated into three regions: the northern
169 extratropics, the southern subtropics-to-midlatitudes, and the southern high-latitudes in section
170 3.3. Lastly, we conclude in section 4.

171

172 **2. Regional SST Biases and Experiment Design**

173 The atmospheric model employed in this study is GFDL AM2.1 (GFDL Global Atmospheric
174 Model Development Team 2004), with 24 vertical levels and a horizontal resolution of 2°
175 latitude × 2.5° longitude. We integrate AM2.1 with the monthly SSTs prescribed to either the
176 observation (NOAA OI SST V2 data; Reynolds et al. 2002) or those from the historical
177 integration of the corresponding coupled model, GFDL CM2.1 (Delworth et al. 2006), both of
178 which are averaged for the period 1982-2000. The former represents the perfect model without

any SST biases while SST biases are present globally in the latter. In all simulations, we prescribe the sea-ice concentration to its monthly climatology averaged between 1982 and 2000 from AMIP2 observational estimates supplied by the Program for Climate Model Diagnosis and Intercomparison (PCMDI). The prescribed SST experiments are integrated for 50 years, and the first 10 years are discarded as a spin-up. Figure 1a illustrates the climatological SST bias of CM2.1, the difference from the observed NOAA SST data. Three features stand out: 1) prominent cold bias in the northern extratropics, 2) zonally elongated cold and warm biases in the southern subtropics and the Southern Ocean, respectively, and 3) tropical-wide cold bias with a strip of warm bias in the eastern ocean basins near the coast. These features are robust, shared by two-thirds of CMIP5/6 models (stippling in Fig. 1a), as noted in previous literature (e.g., Wang et al. 2014; Xiang et al. 2017). The global SST bias of CM2.1 (Figure 1a) and that of the multi-model mean of CMIP5/6 models (Figures S1a and S1b) are strongly correlated at 0.99. This suggests that the SST bias pattern from CM2.1 is representative of that from the current generation of global climate models.

We intend to disentangle the effect of these regional SST biases on the tropical precipitation. For this purpose, we obtain the q-flux that aims to reproduce the climatological SST pattern from either the observation or the model CM2.1. Specifically, the q-flux is calculated as the monthly climatology of net surface heat flux in the aforementioned prescribed SST simulations. The q-flux that reproduces the observed SST is denoted as Q_{OBS} and that reproducing the model SST as Q_{MODEL}. The difference between Q_{MODEL} and Q_{OBS} is denoted as Q_{BIAS} (Figure 1b). While our experiment setting does not point to the root cause of Q_{BIAS}, it should ultimately stem from errors in parameterizations of subgrid-scale physics and its interactions with the large-scale flow.

We prescribe the q-flux profiles to AM2.1 coupled to a 50-m slab ocean, in which the lower boundary includes realistic land-sea distributions and topography. The slab ocean simulation forced by Q_{OBS} represents the perfect model climate with no SST bias (OBS) while the one forced by Q_{MODEL} represents the model climate with the SST biases around the entire globe (GLO). The slab ocean simulations do not perfectly reproduce the corresponding fixed SST simulations, possibly because the air-sea interactions at a frequency higher than monthly are neglected by prescribing the monthly q-flux. However, it is worth noting that the SST deviations in GLO and OBS from their corresponding prescribed SST simulations are similar in spatial pattern and magnitude (Figure S2), indicative of common model errors. Consequently, the SST difference between GLO and OBS (Figure S1c) closely matches the actual SST bias (Figure 1a) and hence the precipitation biases are broadly reproduced by the slab ocean simulations (contrast Figures 1c and 1d). Although non-negligible differences exist over the South Indian Ocean, the Maritime Continent, and the equatorial Atlantic, the pattern correlation between the actual precipitation bias and that reproduced from GLO reaches 0.71 in the Pacific basin between 15°S-15°N, which is our study area. This confirms that the slab ocean simulations can be used for assessing the causes of the tropical Pacific precipitation bias.

In order to disentangle the effect of regional SST biases, we take into account a series of q-flux profiles, formulated as different combinations of Q_{OBS} and Q_{MODEL}. For example, the slab ocean simulation with Q_{MODEL} between 20°S and 20°N and Q_{OBS} over the rest of the globe is intended to examine the effect of tropical SST bias (denoted TRO). We further decompose the tropical bias into the zonally averaged component ([TRO]) and the departure from the zonal average (TRO*). As details set out in Table 1, additional experiments are performed to single out the SST bias in the extratropics (EXT), the northern extratropics (EXT-N), and the southern extratropics (EXT-S) divided into equatorward (EXT-SEQ) and poleward (EXT-SPO) of 40°S,

as seen in Figure 1b. We divide the southern extratropics relative to 40°S because the SST bias (Figure 1a) and hence q-flux changes sign there (Figures 1b and S3). The sum of the climate response in all regional q-flux simulations closely resembles the climate response in GLO (Figure S4). This near-linearity of the climate responses allows us to adopt the regional q-flux simulations for the attribution of the tropical precipitation biases. All slab ocean experiments are integrated for 30 years after 20 years of spin-up. We regard the slab ocean OBS simulation as the observation and hence the difference from OBS defines the climate bias (i.e., experiment minus OBS), denoted by the δ notation.

We emphasize that the aim of this study is to evaluate the contribution of regional SST biases to the double-ITCZ bias pattern. The root cause of regional SST biases can only be speculated with reference to previous studies. For example, the cold bias in the northern tropical East Pacific in TRO may be partially attributable to the low biased orography over Central America that leads to overly strong easterlies (Baldwin et al. 2021). The equatorial cold bias in [TRO] is likely to result from errors in cloud fraction over the equatorial Pacific (Li and Xie 2012; Wittenberg et al. 2006) and erroneous representation of equatorial upwelling, which may originate from models' inability to constrain the extratropical SST (Burls et al. 2017) or turbulent mixing in the upper equatorial ocean (Moum et al. 2013). The warm bias off the west coast of South America in TRO* and EXT-SEQ are attributed to underestimated stratus cloud cover (Ma et al. 1996), weak coastal upwelling (Large and Danabasoglu 2006), and the low biased Andes orography (Takahashi and Battisti 2007). The Southern Ocean warm bias in EXT-SPO may be due to the insufficient supercooled cloud liquid amount (Kay et al. 2016) and the southern subtropical cold bias in EXT-SEQ may be due to overly bright tropical low clouds (Nam et al. 2012), which respectively causes positive and negative biases in the top-of-atmosphere shortwave cloud radiative effects (SWCRE). Indeed, the SWCRE bias features a

dipole structure in the southern extratropics in multiple atmosphere-only models participating in the Fifth and Sixth phase of AMIP (Figure 2), implying that the origin of the southern extratropical biases in CMIP5/6 models (Figure S1a,b) partly lies within the atmospheric model component. The northern extratropical cold bias in EXT-N may be related to too weak oceanic vertical mixing (Zhu et al. 2020), and/or cloud biases (Figure 2).

To examine the large-scale energetics control on the double-ITCZ bias, we calculate the net energy input to the atmospheric column over the equatorial region between 5°S-5°N (NEI_0) and the cross-equatorial atmospheric energy transport (AET_0). Assuming a negligible energy storage in the annual-mean, NEI is calculated as the sum of downward net radiative fluxes at the top-of-atmosphere and upward net heat fluxes at the surface. We calculate AET_0 by integrating the global-mean removed NEI over the Southern Hemisphere (SH). Note that the global mean is removed to ensure that the fluxes vanish at both poles.

We use the equatorial precipitation index (E_p), defined as the equatorial (2°S-2°N) precipitation divided by the tropical mean (20°S-20°N) minus one (Adam et al. 2016), to quantify the hemispherically symmetric component of the zonal-mean double-ITCZ bias. Negative δE_p indicates an excessive precipitation off the equator and an underestimated equatorial precipitation. The anti-symmetric component is measured by the precipitation centroid (p_cent), defined as the centroid latitude that renders an equal area-integrated precipitation from 20°S to 20°N (Frierson and Hwang 2012). Negative δp_cent indicates more precipitation to the south than north of the equator.

3. Results

3.1. Tropical vs extratropical contribution

The CM2.1 presents deficient equatorial and excessive off-equatorial precipitation, with $\delta E_{\mathrm{p}} = -0.11$ which is closely reproduced in GLO where $\delta E_{\mathrm{p}} = -0.12$ (Figures 3f and 4a). The E_{p} bias amounts to -0.14 in TRO and 0.05 in EXT, suggestive of the tropical origin of the hemispherically symmetric bias, consistent with Adam et al. (2016). A large negative E_{p} bias in TRO is due to the negative equatorial Q_{BIAS} by design (Figures 1b and S3) since the symmetric component is related to NEI_0 (Figure 4a). It is of interest to note that the E_{p} bias is significant and positive in EXT despite zero equatorial Q_{BIAS} therein, as the warm Q_{BIAS} effect off the west coast of Chile extends into the southeastern tropical Pacific (Figure 3b; see section 3.3 for details).

The hemispherically anti-symmetric component of $\delta p_{\mathrm{cent}} = -1.3°$ in CM2.1 is also well reproduced by GLO where $\delta p_{\mathrm{cent}} = -1.2°$, indicative of more precipitation in the southern than the northern tropics (Figure 4b). The p_{cent} bias in GLO is largely driven by EXT wherein $\delta p_{\mathrm{cent}} = -1.0°$ while the TRO-induced p_{cent} bias of $0.1°$ is insignificant. In the GFDL model we consider in this study, Q_{BIAS} (Figure 1b) presents a strong hemispheric asymmetry in the extratropics (i.e., poleward of 20°) (Figure S3). The north-minus-south Q_{BIAS} amounts to -0.22 PW poleward of 20° (i.e., 20°N-90°N minus 20°S-90°S) and 0.09 PW equatorward of 20° (i.e., 0°-20°N minus 0°-20°S). More energy input into the southern than the northern hemisphere in EXT results in an anomalously northward cross-equatorial atmospheric energy transport ($\delta \mathrm{AET}_0$), leading to the southward-displaced tropical precipitation (i.e., negative δp_{cent}; Figure 4b). It is noted that the extratropical Q_{BIAS} induces δp_{cent} via modifying the tropical SST, as suggested by the near-perfect correlation between δp_{cent} and δSST difference between 0°-20°N and 0°-20°S, a measure of the tropical SST asymmetry (Figure S5; Hawcroft et al. 2018; Xiang et al. 2018; Kawai et al. 2021). That is, the extratropical Q_{BIAS} would be unable to perturb p_{cent} if it were not allowed to induce any tropical SST changes.

297 The dominance of extratropical impact on the hemispherically anti-symmetric component is
298 consistent with Hwang and Frierson (2013) and Li and Xie (2014).

299 The longitude-latitude structure of the tropical precipitation bias reveals rich spatial patterns
300 embedded in the zonal-mean (Figures 1c and 1d). The double-ITCZ bias is characterized by
301 the dry bias over the western Pacific (WP), the northward shifted precipitation over the northern
302 ITCZ region (NI), and the zonally elongated wet bias over the southern tropics, covering the
303 southeastern Pacific (SEP) and the South Pacific Convergence Zone (SPCZ) regions. The
304 majority of this double-ITCZ bias is reproduced in TRO (Figure 3d). The pattern correlation
305 with the tropical precipitation bias in GLO (Table 1) clearly indicates that the tropical bias is
306 the key for the formation of the overall double-ITCZ bias pattern. The tropical SST bias is
307 characterized by an equatorially elongated cold tongue bias, the northern/southern tropical
308 Pacific warm/cold bias, an overall cold bias in the tropical Atlantic, and a narrow strip of strong
309 warm bias along the west of coastlines (Figure 3a). The region of warm bias displays excessive
310 precipitation, and the region of cold bias displays deficient precipitation (Figure 3d), known as
311 the warmer-get-wetter mechanism (Xie et al. 2010). These tropically-induced biases in SST
312 and precipitation, particularly in the Pacific sector, are partially offset by the extratropically-
313 induced biases (Figures 3b and 3e). That is, the extratropical contribution acts to mitigate the
314 locally driven biases, except over the southeastern Pacific (SEP) where the wet bias is induced
315 by both tropical and extratropical biases (Figures 3d and 3e). Relatedly, the warm bias off the
316 Peruvian coast is evident in both TRO and EXT (Figures 3a and 3b). Thus, the extratropical
317 SST bias correction may reduce the SEP wet bias while worsening the precipitation bias over
318 other tropical regions.

319

3.2. Contrasting the effect of zonally symmetric and asymmetric components of tropical bias

In the previous section, we show that the spatial structure of double-ITCZ is due in large part to the tropical Q_{BIAS}. Noting that the tropical bias features a widespread cold bias (Figure 3a), we decompose the tropical Q_{BIAS} into the zonal average and the deviation from the zonal average. The experiment forced by the zonally uniform Q_{BIAS} in the tropics is denoted as [TRO] and that forced by the zonally asymmetric component as TRO* (Figure 5a-c). Although the amplitude of regional q-flux in [TRO] amounts to only a quarter of that in TRO* (Figure 5a,b), the zonal-mean biases in SST and precipitation are mostly caused by [TRO] (Figure 5f,i). Free of zonal-mean q-flux in TRO*, the cross-equatorial atmospheric energy transport response $\delta \mathrm{AET}_0$ and the atmospheric net energy input response at the equator $\delta \mathrm{NEI}_0$ nearly vanish (Figure 4) and thus TRO* has little impact on the zonal-mean precipitation bias (Figure 5f,i).

The prescribed q-flux in [TRO] is to cool the surface in the deep tropics within ~5° latitude (Figure 5a). Hence, $\delta \mathrm{NEI}_0$ is negative, resulting in an equatorial dry bias, that is, $\delta E_{\mathrm{p}} < 0$ (Figures 4a and 5i), consistent with Adam et al. (2016). Despite the zonally uniform q-flux in [TRO], the resulting tropical cold SST bias is more pronounced in the eastern than the western Pacific basin. This zonal asymmetry in the tropical Pacific SST response results from the distinct SST-surface shortwave flux feedback (Lin 2007) and the evaporative damping rate (Xie et al. 2010) over the warm pool and the cold tongue. The western Pacific is a deep convective regime where reduced SSTs tend to inhibit deep convection and the resulting reduction in clouds allows for more surface downward shortwave radiation. On the contrary, the eastern Pacific is a shallow convective regime where reduced SSTs tend to increase the low cloud amount via an enhanced static stability in the boundary layer (Klein and Hartmann 1993), which in turn decreases the surface downward shortwave radiation. The negative SST-surface

shortwave flux feedback over the western Pacific mutes the SST response while the positive SST-surface shortwave flux feedback over the eastern Pacific amplifies the SST response (contours in Figure 5d). In fact, the shortwave response is partly compensated for by the longwave component. For example, the shortwave heating induced by reduced clouds is partly counteracted by the longwave cooling associated with the enhanced outgoing longwave radiation. However, the cloud radiation response is dominated by the shortwave component in GFDL AM2 (Kang et al. 2014). Additionally, the evaporative damping rate is proportional to the climatological evaporation so that the SST response to the same q-flux is locally enhanced over the climatologically-colder eastern than the climatologically-warmer western equatorial Pacific. A consequently enhanced trade easterlies give rise to anomalous equatorial divergence, reducing precipitation over the warm pool while shifting the northern ITCZ northward and the SPCZ southward (Figure 5g).

Despite a small zonal-mean response in TRO* (Figure 5f,i), the regional precipitation responses are as large as that in [TRO] (compare Figures 5g and 5h). While an overall tropical cooling is associated with the zonally uniform Q_{BIAS} (Figure 5d), the warm biases over the northern tropical Pacific and the west coast of America and Africa are associated with the zonally asymmetric Q_{BIAS} (Figure 5e). The northern tropical Pacific warm bias acts to displace the northern ITCZ (NI) northward, intensifying the precipitation bias over the NI region associated with the equatorial cold bias (Figure 5g,h). The warm bias off the west coast of South America is concentrated in a narrow strip (Figure 5e), but its magnitude is large enough to induce a large-scale convergence, leading to the wet bias extending from the Peruvian coast to the southeastern Pacific (SEP) region (Figure 5h). The dry bias over the western Pacific in TRO* is associated with the relative cooling over the warm pool. In sum, TRO* is equally important as [TRO] for shaping the regional precipitation pattern bias (Figure 5g,h) despite the

negligible zonal-mean precipitation bias with nearly zero δE_{p} and δp_{cent} (Figure 4). In fact, the pattern correlation with the GLO response is slightly larger in TRO* than in [TRO] (Table 1).

3.3 Decomposition of extratropical contribution

We show in section 3.1 that the tropical Q_{BIAS} is most responsible for developing an overall double-ITCZ bias but the hemispherically asymmetric component of zonal-mean precipitation bias (i.e., δp_{cent}) is in large part driven by the extratropical biases. Hwang and Frierson (2013) suggest that the typically underestimated cloud cover in the Southern Ocean makes the SH warmer than the NH, inducing an anomalous Hadley cell that drives a northward cross-equatorial atmospheric energy transport (AET_0), which then leads to excessive precipitation to the south of the equator. GFDL CM2.1 shows the same tendency of warm bias poleward of 40°S and this is flanked by cold biases on the equatorward side (Figures 1a). This dipole structure is also evident in the previous version of the model CM2.0 (Delworth et al. 2006).

Given the coexistence of the warm and cold biases in the southern extratropics, we separate their effects by running the experiments with Q_{BIAS} prescribed over either 20°S-40°S (EXT-SEQ) or poleward of 40°S (EXT-SPO). Consistent with the energetics framework, the warm bias poleward of 40°S results in a negative δp_{cent} (i.e., a southward shift of the precipitation centroid) in EXT-SPO while the cold bias over 20°S-40°S results in a positive δp_{cent} (i.e., a northward shift of the precipitation centroid) in EXT-SEQ (Figure 4b). Due to the cancelling effect, the southern extratropical bias as a whole (i.e., poleward of 20°S; EXT-S) has an insignificant impact on the δp_{cent}. Although previous literature has emphasized the southern high-latitude warm bias for displacing the zonal-mean ITCZ southward (e.g., Hwang and

391 Frierson 2013), this study highlights the compensating effect by the neighboring cold bias in
392 the southern mid-latitude, at least in a portion of CMIP5/6 models (Figure 2). Importantly, the
393 near zero impact of EXT-S on both the hemispherically symmetric and asymmetric
394 components of the zonal-mean diagnostics (i.e., δE_{p} and δp_{cent}) does not necessarily
395 indicate that it is unimportant for the double-ITCZ bias. The southern extratropical biases in
396 EXT-S are considerably responsible for the zonally elongated wet bias south of the equator
397 while partially alleviating the precipitation biases over the western Pacific (WP) and the
398 northern ITCZ (NI) regions (contrast Figures 6g and 1c). This demonstrates the limitations of
399 the zonal mean framework and highlights the importance of assessing regional variations of
400 the precipitation.

401 The negative δp_{cent} in EXT-SPO is a manifestation of a southward precipitation shift in
402 all tropical regions except the southeastern Pacific (SEP) (Figure 6e). It is noteworthy that the
403 southern high-latitude warm bias is not responsible for the SEP wet bias in GLO. Instead, the
404 SEP wet bias appears in EXT-SEQ (Figure 6f) associated with a narrow strip of warm bias
405 extending into the Peruvian coast (Figure 6b), which results from the positive Q_{BIAS} off the
406 Chilean coast (Figure 1b). The separation of EXT-SEQ and EXT-SPO, together with TRO*,
407 clearly demonstrates that the SEP wet bias is driven by the local warm bias due to model errors
408 in regional processes. The northward precipitation shifts in the western Pacific (WP) and SPCZ
409 in EXT-SEQ are consistent with the energetics framework (Figure 6f). However, the northern
410 ITCZ (NI) region presents a reversed precipitation shift associated with the evident cooling in
411 the northeastern tropical Pacific (Figure 6b). The intensification of the north Pacific subtropical
412 high, induced by the propagation of southern extratropical cold bias, results in anomalous
413 northeasterlies over the eastern tropical Pacific, forming a cold temperature anomaly via the

414 wind-evaporation-SST (WES) feedback and shifting the precipitation equatorward in the NI
415 region.

416 Meanwhile, the Northern Hemisphere shows clear cold biases in the extratropics (Figure 1a),
417 The experiment with the prescribed Q_{BIAS} poleward of 20°N (i.e., EXT-N) is to examine the
418 effect of the northern extratropical cold bias in isolation. Anomalously northward cross-
419 equatorial atmospheric energy transport (AET_0) leads to a southward shift of the zonal-mean
420 tropical precipitation, indicated by a negative δp_{cent} (Figure 4b). The large negative δp_{cent}
421 is a result of the overall wet bias in the southern tropics and the southward-displaced northern
422 ITCZ (Figure 6h). The northern extratropical cold bias is advected equatorward, but the cooling
423 response is limited to the north of the equator due to the blocking effect by the mean ITCZ
424 (Figure 6d; Kang et al. 2020). A contrast with EXT-S clearly highlights the limited ability of
425 the northern extratropical bias in affecting the SSTs of the opposite hemisphere (Figures 6c vs
426 6d). The northern extratropical signal in EXT-N penetrates across the equator only through the
427 western Pacific warm pool where deep convection is organized around the equator (Kang et al.
428 2020). The resultant cold bias around the SH maritime continents acts to shift the SPCZ
429 precipitation northeastward. This is consistent with a southward SPCZ shift in response to the
430 northern extratropical warming in Kang et al. (2018). Owing to the dipole pattern in the
431 southern extratropical SST biases, the northern extratropical cold bias turns out to be more
432 critical at causing a southward shift of the zonal-mean tropical precipitation (Figure 4b).
433 Although δp_{cent} points to the dominant role of the northern extratropical cold bias in forming
434 the double-ITCZ bias (Figure 4b), the regional variations indicate that EXT-S and EXT-N are
435 comparably responsible for the tropical Pacific response (Figures 6g and 6h). It is the Indian
436 Ocean response of opposite sign that diminishes δp_{cent} in EXT-S. A northward precipitation
437 shift over the Indian Ocean in EXT-S, driven by the cold bias over the southern Indian Ocean

438 in EXT-SEQ (Figure 6f), counteracts a southward precipitation shift at other ocean basins. As
439 with the southern extratropical biases, fixing the northern extratropical cold bias would only
440 worsen the northern ITCZ bias but partially mitigates the southern tropical wet bias.

441

442 **4. Conclusions**

443 The primary focus of this study is to examine how the regional SST bias is manifest in the
444 double-ITCZ bias. We use one GFDL model, CM2.1, but presume our results to be generally
445 applicable to other models as the global SST and tropical precipitation bias patterns in CM2.1
446 are largely common to those in the current generation of global climate models. The experiment
447 with SSTs prescribed to the observation is first conducted to infer the monthly q-flux that is
448 used to force the slab ocean to replicate the observed SSTs. The same procedure is repeated
449 but with the SSTs prescribed to the model CM2.1. The q-flux difference between the two
450 prescribed SST experiments is denoted as Q_{BIAS}, which reproduces the global SST bias via the
451 slab ocean model. The slab ocean experiments are limited in perfectly reproducing the actual
452 SST biases in a fully coupled model, possibly suggesting the need to account for the air-sea
453 interactions at a frequency higher than monthly. However, the slab ocean model simulates the
454 SST biases broadly similar in spatial distributions to our target model CM2.1 (Figure 1a vs
455 S1c), confirmed by the pattern correlation of 0.94 between 30°S-30°N. We further confirm the
456 linearity of the climate response to the regional Q_{BIAS}, hence, allowing us to decompose biases
457 in the climate system to the contributions from the regional Q_{BIAS}.

458 In particular, we single out the effect of the northern extratropical cold bias, the Southern
459 Ocean warm bias, the southern mid-latitude cold bias, and the tropical cold bias. Previous
460 literature raised a possibility of the Southern Ocean warm bias for causing the southward-

displaced zonal-mean ITCZ in coupled models. However, the Southern Ocean warm bias effect in CM2.1 is cancelled out by the southern mid-latitude cold bias effect. This pair of opposite-signed extratropical biases in the Southern Hemisphere is evident in a portion of CMIP5/6 models (Figure 2). Our experiments suggest the northern extratropical cold bias is responsible for the hemispherically asymmetric bias in the zonal-mean ITCZ. However, the examination of regional variations indicates that the northern extratropical cold bias and the dipole-structured southern extratropical bias have a comparable contribution to the tropical Pacific precipitation response. The extratropical Q_{BIAS} in both hemispheres is considerably responsible for the wet bias south of the equatorial Pacific but it counterintuitively ameliorates the precipitation bias over the northern tropical Pacific.

Therefore, the zonally averaged precipitation diagnostics, such as the equatorial precipitation index E_{p} and the precipitation centroid index p_{cent}, have limited relevance for local precipitation. Hence, caution must be taken when the energetics framework is invoked to understand the regional precipitation response (Atwood et al. 2020; Mamalakis et al. 2021). The zonal-mean diagnostics poorly represent the tropical Pacific bias as indicated by an examination of the longitude-latitude structure. For example, the zonally asymmetric tropical bias (i.e., TRO*) has little impact on the zonal-mean tropical precipitation pattern as a result of the cancellation between a large drying response over the equatorial Pacific and a large wetting response over other ocean basins. Hence, the zonally asymmetric tropical bias is as critical as the zonally symmetric tropical bias for shaping the tropical Pacific precipitation bias. Moreover, the factors responsible for a southward zonal-mean ITCZ shift such as the cold northern extratropical bias and the warm Southern Ocean bias turn out be irrelevant to the wet bias over the southeastern Pacific, which instead is driven by the narrow strip of warm bias along the west coast of South America. Additionally, although the hemispherically asymmetric

485 component of the zonal-mean tropical precipitation bias, estimated from the precipitation
486 centroid, is primarily driven by the extratropical biases, an overall tropical Pacific bias pattern
487 largely originates from the tropical biases (Figures 1c vs 3d,e). In fact, a better representation
488 of extratropical processes will hinder the improvement of the northern tropical Pacific
489 precipitation bias. The extratropical biases as a whole shift the northern ITCZ equatorward and
490 cause a wet bias in the southeastern Pacific, so that ironically the extratropical bias correction
491 will intensify the northern tropical Pacific precipitation bias while partially ameliorating the
492 southern tropical Pacific bias. These instances clearly show that regional bias corrections may
493 bring about unintended remote impacts, highlighting the compounding nature of model tuning
494 procedures to reduce biases.

495 Precisely speaking, Q_{BIAS} is not necessarily the surface heat flux bias itself but encompasses
496 the effect of uncertainties in the subgrid-scale parameterizations on the SST. While the origins
497 of regional SST biases are beyond the scope of this study, the proposed causes are reviewed in
498 section 2. A major caveat of this study is omission of ocean dynamical feedbacks, which not
499 only damps the magnitude but also modulates the spatial pattern of tropical climate response
500 to radiative forcing (e.g., Kang et al. 2020). The negative ocean dynamical feedback is shown
501 to be stronger for extratropical than for tropical radiative perturbations (Green et al. 2019; Yu
502 and Pritchard 2019), so that the importance of the northern extratropical cold bias in causing
503 the southward-displaced zonal-mean ITCZ may be over-emphasized in our experiments.
504 Furthermore, we note that while our slab ocean configuration is successful in reproducing the
505 tropical Pacific biases of a corresponding coupled model, there exist non-negligible deviations
506 at other ocean basins. However, the study provides a useful guidance for where should be
507 targeted to improve particular features of climatological precipitation biases. A subsequent

508 study with a fully atmosphere-ocean coupled model is warranted to examine how the results
509 reported here are modulated by ocean dynamics.

510

511 **References**

512 Adam O, Schneider T, Brient F, Bischoff T (2016) Relation of the double-ITCZ bias to the
513 atmospheric energy budget in climate models. Geophys Res Lett 43:7670-7677.
514 https://doi.org/10.1002/2016GL069465

515 Atwood AR, Donohoe A, Battisti DS, Liu X, Pausata FSR (2020) Robust Longitudinally
516 Variable Responses of the ITCZ to a Myriad of Climate Forcings. Geophys Res Lett, 47,
517 e2020GL088833, https://doi.org/10.1029/2020GL088833.

518 Baldwin JW, Atwood AR, Vecchi GA, Battisti DS (2021) Outsize Influence of Central
519 American Orography on Global Climate. AGU Advances 2.
520 https://doi.org/10.1029/2020AV000343

521 Bellucci A, Gualdi S, Navarra A (2010) The Double-ITCZ Syndrome in Coupled General
522 Circulation Models: The Role of Large-Scale Vertical Circulation Regimes. J Clim 23:1127–
523 1145. https://doi.org/10.1175/2009JCLI3002.1

524 Bischoff T, Schneider T (2016) The Equatorial Energy Balance, ITCZ Position, and Double-
525 ITCZ Bifurcations. J Clim 29:2997–3013. https://doi.org/10.1175/JCLI-D-15-0328.1

526 Burls NJ, Muir L, Vincent EM, Fedorov A (2017) Extra-tropical origin of equatorial Pacific
527 cold bias in climate models with links to cloud albedo. Clim Dynam 49:2093–2113.
528 https://doi.org/10.1007/s00382-016-3435-6

529 De Szoeke SP, Xie SP (2008) The Tropical Eastern Pacific Seasonal Cycle: Assessment of
530 Errors and Mechanisms in IPCC AR4 Coupled Ocean–Atmosphere General Circulation
531 Models. J Clim 21:2573–2590. https://doi.org/10.1175/2007JCLI1975.1

532 Delworth TL, Broccoli AJ, Rosati A, et al (2006) GFDL's CM2 Global Coupled Climate
533 Models. Part I: Formulation and Simulation Characteristics. J Clim 19:643–674.

534 https://doi.org/10.1175/JCLI3629.1

535 Frierson DMW, Hwang YT (2012) Extratropical Influence on ITCZ Shifts in Slab Ocean
536 Simulations of Global Warming. J Clim 25:720–733. https://doi.org/10.1175/JCLI-D-11-
537 00116.1

538 Fushan D, Rucong Y, Xuehong Z, et al (2005) Impacts of an improved low-level cloud scheme
539 on the eastern Pacific ITCZ-cold tongue complex. Adv Atmos Sci 22:559–574.
540 https://doi.org/10.1007/BF02918488

541 GFDL Global Atmospheric Model Development Team (2004) The New GFDL Global
542 Atmosphere and Land Model AM2–LM2: Evaluation with Prescribed SST Simulations. J Clim
543 17:4641–4673. https://doi.org/10.1175/JCLI-3223.1

544 Green B, Marshall J, Campin J-M (2019) The 'sticky' ITCZ: ocean-moderated ITCZ shifts.
545 Clim Dyn 53:1–19. https://doi.org/10.1007/s00382-019-04623-5

546 Guilyardi E, Delecluse P, Gualdi S, Navarra A (2003) Mechanisms for ENSO Phase Change
547 in a Coupled GCM. J Clim 16:1141-1158. https://doi.org/10.1175/1520-
548 0442(2003)16<1141:MFEPCI>2.0.CO;2

549 Ham YG, Kug JS (2014) Effects of Pacific Intertropical Convergence Zone precipitation bias
550 on ENSO phase transition. Environ Res Lett 9:064008. https://doi.org/10.1088/1748-
551 9326/9/6/064008

552 Hawcroft M, Haywood JM, Collins M, et al (2017) Southern Ocean albedo, inter-hemispheric
553 energy transports and the double ITCZ: global impacts of biases in a coupled model. Clim Dyn
554 48:2279–2295. https://doi.org/10.1007/s00382-016-3205-5

555 Hawcroft M, Haywood JM, Collins M, and Jones A (2018) The contrasting climate response
556 to tropical and extratropical energy perturbations. Clim Dyn 51:3231–3249.
557 https://doi.org/10.1007/s00382-018-4076-8

558 Hwang YT, Frierson DMW (2013) Link between the double-intertropical convergence zone
559 problem and cloud biases over the Southern Ocean. Proc Natl Acad Sci USA 110:4935–4940.

https://doi.org/10.1073/pnas.1213302110

Kang SM, Held IM (2012) Tropical precipitation, SSTs and the surface energy budget: a zonally symmetric perspective. Clim Dyn 38:1917–1924. https://doi.org/10.1007/s00382-011-1048-7

Kang SM, Held IM, Frierson DMW, Zhao M (2008) The Response of the ITCZ to Extratropical Thermal Forcing: Idealized Slab-Ocean Experiments with a GCM. J Clim 21:3521–3532. https://doi.org/10.1175/2007JCLI2146.1

Kang SM, Held IM, Xie SP (2014) Contrasting the tropical responses to zonally asymmetric extratropical and tropical thermal forcing. Clim Dyn 42:2033–2043. https://doi.org/10.1007/s00382-013-1863-0.

Kang, SM, Park K, Hwang YT, Hsiao WT (2018) Contrasting Tropical Climate Response Pattern to Localized Thermal Forcing Over Different Ocean Basins. Geophys Res Lett, 45:12,544-12,552. https://doi.org/10.1029/2018GL080697.

Kang SM et al (2019) Extratropical-Tropical Interaction Model Intercomparison Project (ETIN-MIP): Protocol and Initial Results. Bull Am Meteorol Soc 100:2589–2606. https://doi.org/10.1175/ BAMS-D-18-0301.1

Kang SM, Xie SP, Shin Y, et al (2020) Walker circulation response to extratropical radiative forcing. Sci Adv 6:eabd3021. https://doi.org/10.1126/sciadv.abd3021

Kawai H, Koshiro T, Yukimoto S (2021) Relationship between shortwave radiation bias over the Southern Ocean and the double-intertropical convergence zone problem in MRI-ESM2. Atmos Sci Lett. https://doi.org/10.1002/asl.1064

Kay JE, Wall C, Yettella V, et al (2016) Global Climate Impacts of Fixing the Southern Ocean Shortwave Radiation Bias in the Community Earth System Model (CESM). J Clim 29:4617–4636. https://doi.org/10.1175/JCLI-D-15-0358.1

Kim H, Kang SM, Takahashi K, et al (2021) Mechanisms of tropical precipitation biases in climate models. Clim Dynam 56:17–27. https://doi.org/10.1007/s00382-020-05325-z

586 Klein SA, Hartmann DL (1993) The seasonal cycle of low stratiform clouds. J Clim 6:1587-
587 1606. https://doi.org/10.1175/1520-0442(1993)006<1587:TSCOLS>2.0.CO;2

588 Large WG, Danabasoglu G (2006) Attribution and Impacts of Upper-Ocean Biases in CCSM3.
589 J Clim 19:2325–2346. https://doi.org/10.1175/JCLI3740.1

590 Li G, Xie SP (2012) Origins of tropical-wide SST biases in CMIP multi-model ensembles.
591 Geophys Res Lett 39. https://doi.org/10.1029/2012GL053777

592 Li G, Xie SP (2014) Tropical Biases in CMIP5 Multimodel Ensemble: The Excessive
593 Equatorial Pacific Cold Tongue and Double ITCZ Problems. J Clim 27:1765–1780.
594 https://doi.org/10.1175/JCLI-D-13-00337.1

595 Lin JL (2007) The Double-ITCZ Problem in IPCC AR4 Coupled GCMs: Ocean–Atmosphere
596 Feedback Analysis. J Clim 20:4497–4525. https://doi.org/10.1175/JCLI4272.1

597 Lindzen RS, Nigam S (1987) On the role of sea surface temperature gradients in forcing low-
598 level winds and convergence in the tropics. J Atmos Sci 44:2418-2436.
599 https://doi.org/10.1175/1520-0469(1987)044<2418:OTROSS>2.0.CO;2

600 Loeb NG, Doelling DR, Wang H, et al (2018) Clouds and the Earth's Radiant Energy System
601 (CERES) Energy Balanced and Filled (EBAF) Top-of-Atmosphere (TOA) Edition-4.0 Data
602 Product. J Clim 31:895–918. https://doi.org/10.1175/JCLI-D-17-0208.1

603 Ma CC, Mechoso CR, Robertson AW, Arakawa A (1996). Peruvian stratus clouds and the
604 tropical Pacific circulation: A coupled ocean-atmosphere GCM study. J Clim 9:1635-1645.
605 https://doi.org/10.1175/1520-0442(1996)009<1635:PSCATT>2.0.CO;2

606 Mamalakis A et al (2021) Zonally contrasting shifts of the tropical rain belt in response to
607 climate change. Nature Climate Change, https://doi.org/10.1038/s41558-020-00963-x.

608 Mechoso CR et al (1995) The seasonal cycle over the tropical pacific in coupled ocean–
609 atmosphere general circulation models. Mon Weather Rev 123:2825–2838.
610 https://doi.org/10.1175/1520- 0493(1995)123%3c2825:Tscott%3e2.0.Co;2

611 Mechoso CR, Losada T, Koseki S, et al (2016) Can reducing the incoming energy flux over

612 the Southern Ocean in a CGCM improve its simulation of tropical climate?: Southern Ocean-
613 Tropics Link in a CGCM. Geophys Res Lett 43:11,057-11,063.
614 https://doi.org/10.1002/2016GL071150

615 Moum JN, Perlin A, Nash JD, McPhaden MJ (2013) Seasonal sea surface cooling in the
616 equatorial Pacific cold tongue controlled by ocean mixing. Nature 500:64–67.
617 https://doi.org/10.1038/nature12363

618 Nam C, Bony S, Dufresne JL, Chepfer H (2012) The 'too few, too bright' tropical low-cloud
619 problem in CMIP5 models. Geophys Res Lett 39. https://doi.org/10.1029/2012GL053421

620 Oueslati B, Bellon G (2015) The double ITCZ bias in CMIP5 models: interaction between SST,
621 large-scale circulation and precipitation. Clim Dynam 44:585–607.
622 https://doi.org/10.1007/s00382-015-2468-6

623 Reynolds RW, Rayner NA, Smith TM, et al (2002) An Improved In Situ and Satellite SST
624 Analysis for Climate. J Clim 15:1609-1625. https://doi.org/10.1175/1520-
625 0442(2002)015<1609:AIISAS>2.0.CO;2

626 Seager R, Cane M, Henderson N, et al (2019) Strengthening tropical Pacific zonal sea surface
627 temperature gradient consistent with rising greenhouse gases. Nat Clim Change 9:517–522.
628 https://doi.org/10.1038/s41558-019-0505-x

629 Shukla J, DelSole T, Fennessy M, et al (2006) Climate model fidelity and projections of climate
630 change. Geophys Res Lett 33. https://doi.org/10.1029/2005GL025579

631 Takahashi K, Battisti DS (2007) Processes Controlling the Mean Tropical Pacific Precipitation
632 Pattern. Part I: The Andes and the Eastern Pacific ITCZ. J Clim 20:3434–3451.
633 https://doi.org/10.1175/JCLI4198.1

634 Tian BJ (2015) Spread of model climate sensitivity linked to double-Intertropical Convergence
635 Zone bias. Geophys Res Lett 42:4133–4141. https://doi.org/10.1002/2015GL064119

636 Tian BJ, Dong X (2020) The Double-ITCZ Bias in CMIP3, CMIP5, and CMIP6 Models Based
637 on Annual Mean Precipitation. Geophys Res Lett 47. https://doi.org/10.1029/2020GL087232

638 Wang C, Zhang L, Lee S-K, et al (2014) A global perspective on CMIP5 climate model biases.
639 Nature Clim Change 4:201–205. https://doi.org/10.1038/nclimate2118

640 Wittenberg AT, Rosati A, Lau NC, Ploshay JJ (2006) GFDL's CM2 Global Coupled Climate
641 Models. Part III: Tropical Pacific Climate and ENSO. J Clim 19:698–722.
642 https://doi.org/10.1175/JCLI3631.1

643 Xiang B, Zhao M, Held IM, Golaz J (2017) Predicting the severity of spurious "double ITCZ"
644 problem in CMIP5 coupled models from AMIP simulations. Geophys Res Lett 44:1520–1527.
645 https://doi.org/10.1002/2016GL071992

646 Xiang B, Zhao M, Ming Y, et al (2018) Contrasting Impacts of Radiative Forcing in the
647 Southern Ocean versus Southern Tropics on ITCZ Position and Energy Transport in One GFDL
648 Climate Model. Journal of Climate 31:5609–5628. https://doi.org/10.1175/JCLI-D-17-0566.1

649 Xie PP, Arkin PA (1997) Global precipitation: a 17-year monthly analysis based on gauge
650 observations, satellite estimates, and numerical model outputs. Bull Am Meteorol Soc
651 78:2539–2558. https://doi. org/10.1175/1520-0477(1997)078%3c2539:Gpayma%3e2.0.Co;2

652 Xie SP, Deser C, Vecchi GA, et al (2010) Global Warming Pattern Formation: Sea Surface
653 Temperature and Rainfall. J Clim 23:966–986. https://doi.org/10.1175/2009JCLI3329.1

654 Yu S, Pritchard MS (2019) A Strong Role for the AMOC in Partitioning Global Energy
655 Transport and Shifting ITCZ Position in Response to Latitudinally Discrete Solar Forcing in
656 CESM1.2. Journal of Climate 32:2207–2226. https://doi.org/10.1175/JCLI-D-18-0360.1

657 Zhang X, Liu H, Zhang M (2015) Double ITCZ in Coupled Ocean-Atmosphere Models: From
658 CMIP3 to CMIP5. Geophys Res Lett 42:8651–8659. https://doi.org/10.1002/2015GL065973

659 Zheng Y, Shinoda T, Lin JL, Kiladis GN (2011) Sea Surface Temperature Biases under the
660 Stratus Cloud Deck in the Southeast Pacific Ocean in 19 IPCC AR4 Coupled General
661 Circulation Models. J Clim 24:4139–4164. https://doi.org/10.1175/2011JCLI4172.1

662 Zhou ZQ, Xie SP (2015) Effects of Climatological Model Biases on the Projection of Tropical
663 Climate Change. J Clim 28:9909–9917. https://doi.org/10.1175/JCLI-D-15-0243.1

664 Zhu Y, Zhang RH, Sun J (2020) North Pacific Upper-Ocean Cold Temperature Biases in
665 CMIP6 Simulations and the Role of Regional Vertical Mixing. J Clim 33:7523–7538.
666 https://doi.org/10.1175/JCLI-D-19-0654.1
667
668
669
670
671
672
673
674
675
676
677
678
679
680
681
682
683
684
685
686
687

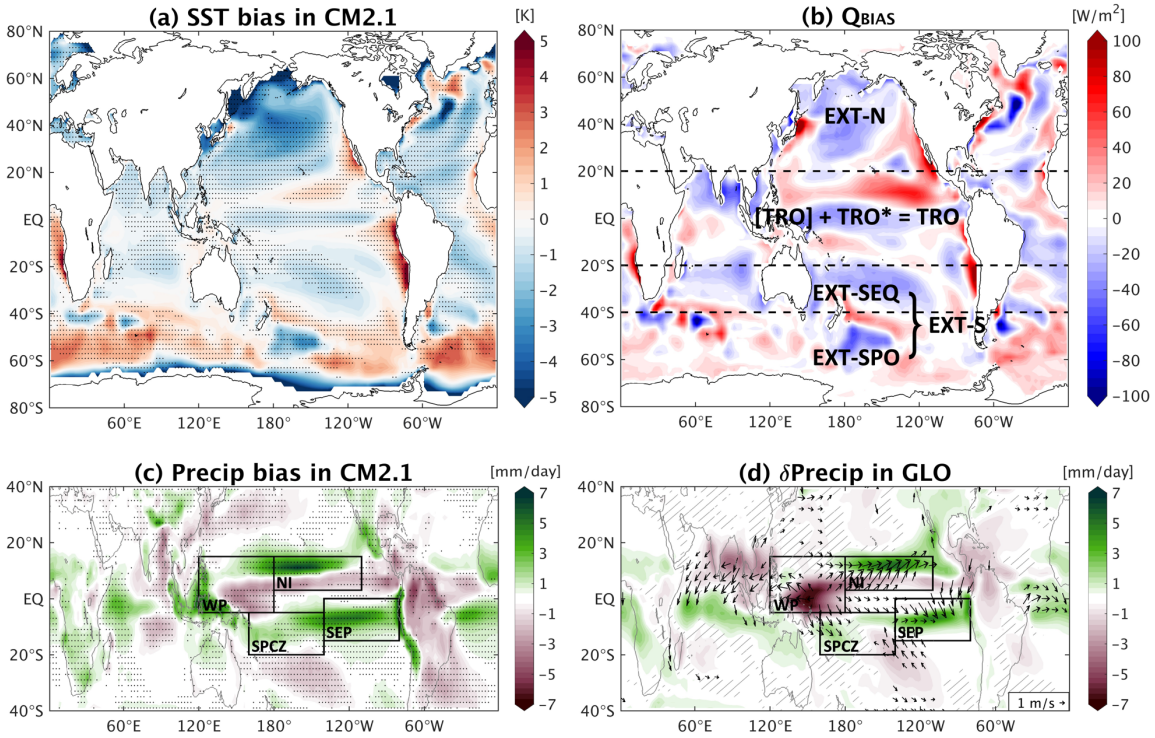

688

689 **Fig. 1** Model biases and fidelity of slab experiments. (a) The climatological SST bias in GFDL
690 CM2.1 relative to NOAA OI SST V2 data. (b) The difference of net surface heat flux (with the
691 sign convention that positive heats the surface) in simulations with the SSTs prescribed to
692 CM2.1 and observation, which is used as the q-flux to force the slab ocean model to reproduce
693 the SST bias shown in (a). The texts in (b) indicate the names of each experiment with a
694 regional Q_{BIAS}. Please refer to Table 1 for details. (c) The climatological tropical precipitation
695 bias in CM2.1, computed as the deviation from Climate Prediction Centre Merged Analysis of
696 Precipitation (CMAP; Xie and Arkin 1997). Stippling in (a) and (c) denotes the regions where
697 more than two-thirds of 41 CMIP5 models and 62 CMIP6 models exhibit the biases with the
698 same sign as CM2.1. (d) The difference of precipitation (shading) and surface wind velocity
699 (vectors) between GLO and OBS. The rectangles in (c) and (d) represent the northern ITCZ
700 (NI), Warm Pool (WP), SPCZ, and southeastern Pacific (SEP). In (d), the regions are hatched
701 where the response is not statistically different from zero at the 99 % confidence level
702 calculated with a two-sided *t*-test.

703

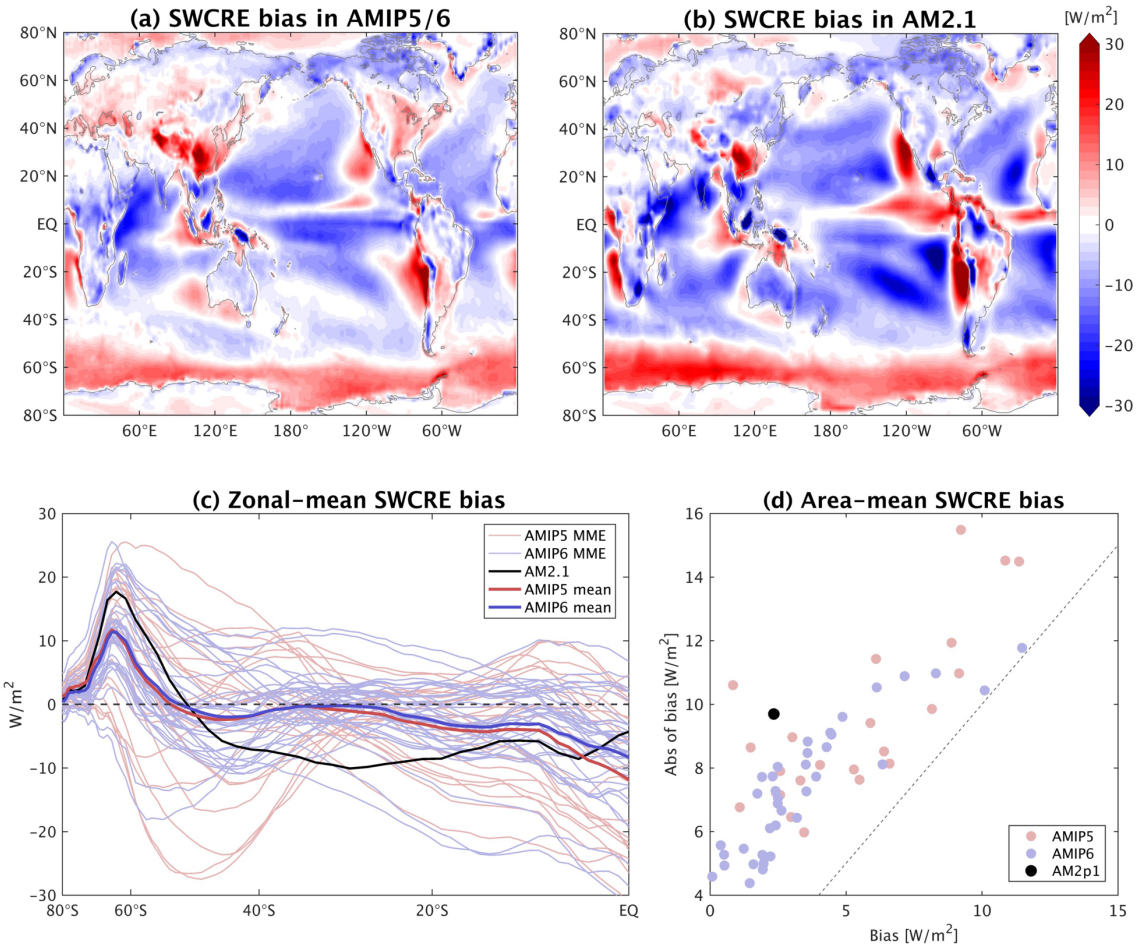

704

705 **Fig. 2** Attribution of the dipole-structured SST bias in the southern extratropics to the dipole-
706 structured SWCRE bias. The top-of-atmosphere SWCRE bias in multi-model ensemble (MME)
707 mean from (a) 24 AMIP5 and 44 AMIP6 models, (b) GFDL AM2.1, and (c) their zonal
708 averages, relative to CERES-EBAF_Ed4.0 data (Loeb et al. 2018) for the period 2000-2018.
709 (d) Comparison of the absolute value of area-averaged SWCRE bias over 20°S~90°S (abscissa)
710 and the area-average of the absolute of SWCRE bias over 20°S~90°S (ordinate). The 1:1 line
711 is indicated by the black dashed. Larger values in the ordinate than in the abscissa indicates a
712 compensation of SWCRE bias within the southern extratropics.

713

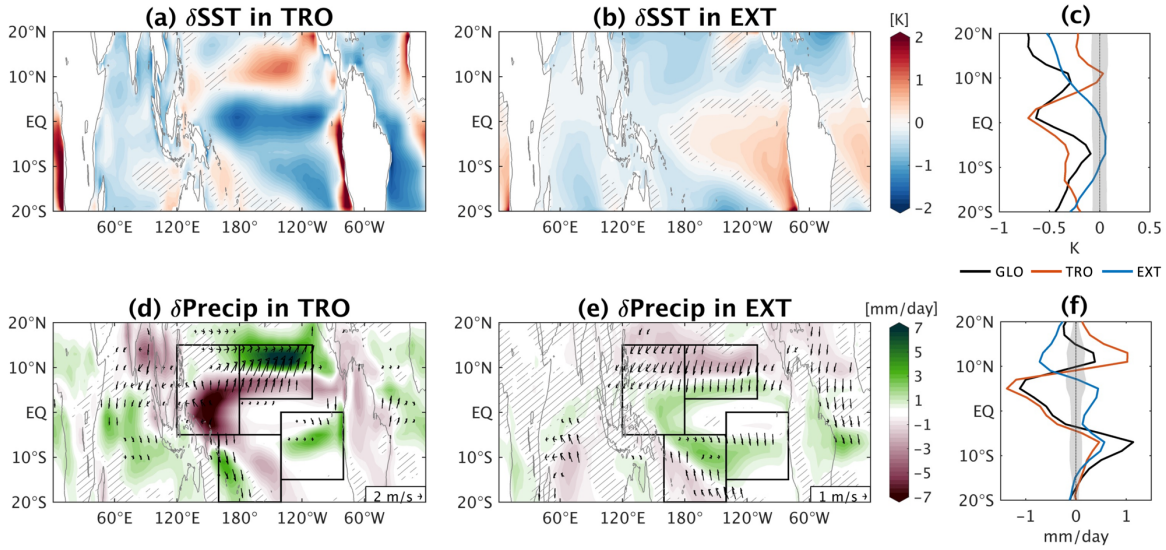

714

715 **Fig. 3** Decomposition of the tropical and extratropical Q_{BIAS} effects. The SST difference
716 between (a) TRO and OBS and (b) EXT and OBS. (d,e) Same as (a,b) but for precipitation and
717 surface wind vector. The zonally averaged difference of (c) SST and (f) precipitation in GLO
718 (black), TRO (red), and EXT (red) from OBS. Hatching in (a,b,d,e) and gray shading in (c,f)
719 indicate where the response is not statistically different from zero at the 99 % confidence level
720 using a two-sided *t*-test.

721

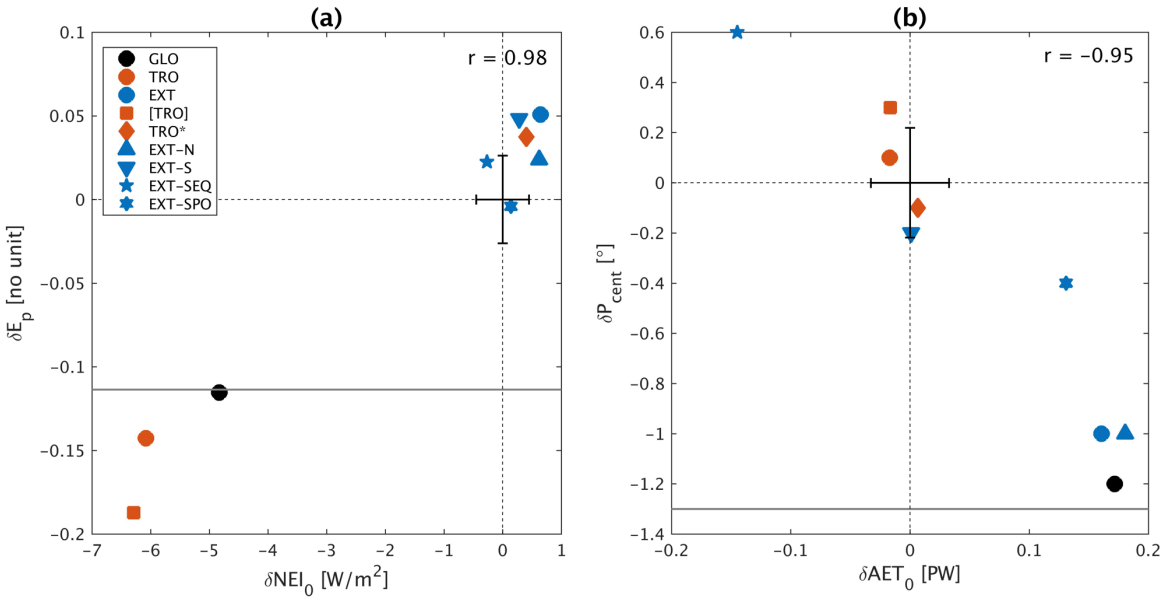

Fig. 4 Energetics and zonal-mean precipitation diagnostics. Scatter diagram of (a) $\delta \mathrm{NEI}_0$ and δE_P and (b) $\delta \mathrm{AET}_0$ and δp_cent for all regional q-flux experiments. The correlation coefficients are displayed in the upper right corner of each panel. A horizontal gray solid line indicates the actual CM2.1 precipitation bias relative to CMAP data (Xie and Arkin 1997). The error bars indicate where the response is not statistically different from zero at the 99 % confidence level using a two-sided *t*-test.

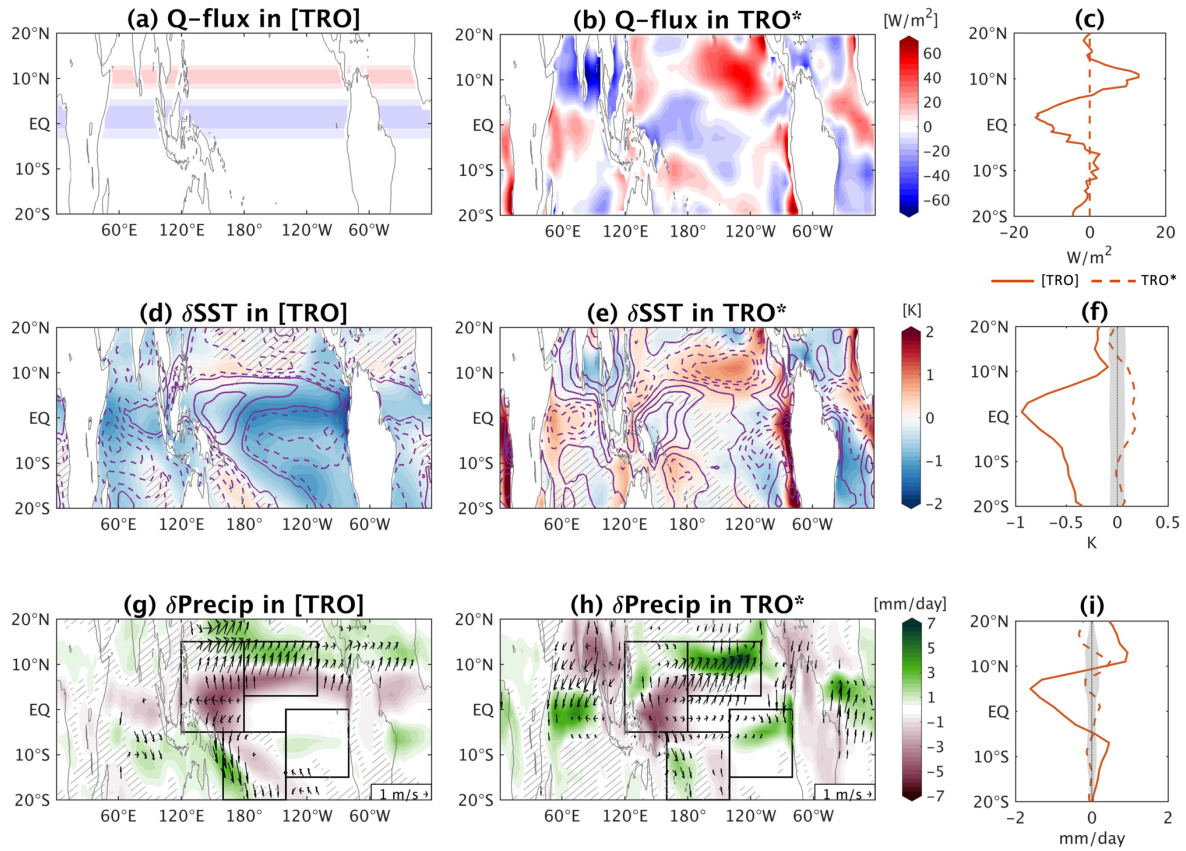

Fig. 5 Decomposition of the tropical Q_{BIAS} effect into the zonally symmetric and asymmetric components. The (top) q-flux profile, the difference of (middle) SST and (bottom) precipitation and surface wind vector from OBS in (left) [TRO] and (right) TRO*. (c,f,i) The corresponding zonal-mean profiles in [TRO] (solid) and TRO* (dashed). Purple solid (dashed) contours in (d,e) denote a positive (negative) response in shortwave cloud radiative effect at the top-of-atmosphere (positive downward; interval = 4 W/m^2). Hatching in (d,e,g,h) and gray shading in (f,i) indicate where the response is not statistically different from zero at the 99 % confidence level using a two-sided *t*-test.

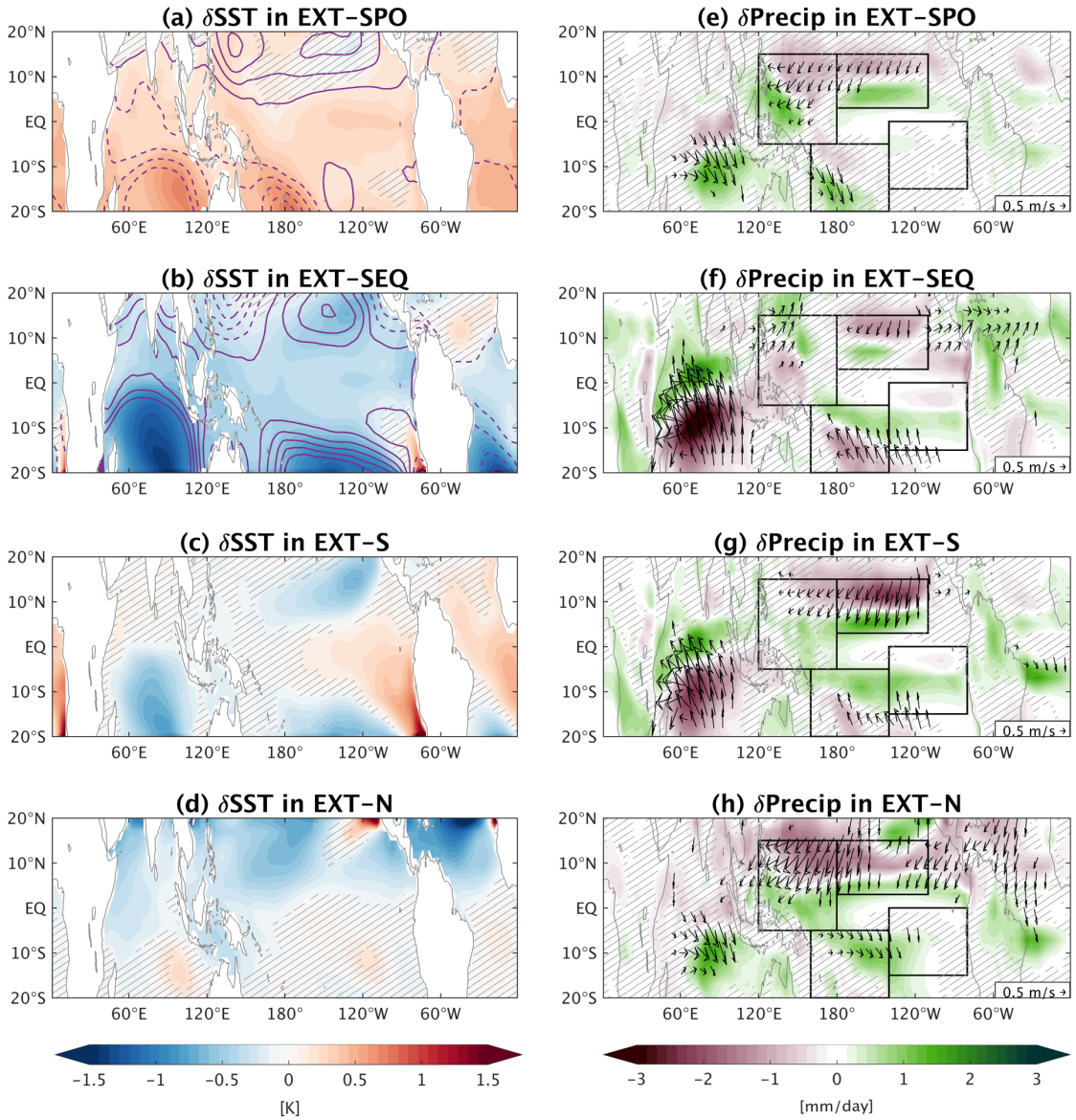

738

739 **Fig. 6** Decomposition of the extratropical Q_{BIAS} effect. The difference of (left) SST and (right)
740 precipitation and surface wind vector from OBS in (a,e) EXT-SPO, (b,f) EXT-SEQ, (c,g) EXT-
741 S, and (d,h) EXT-N. Purple solid (dashed) contour lines in (a,b) denote positive (negative) SLP
742 bias with an interval of 10 Pa. Hatching indicates where the response is not statistically different
743 from zero at the 99 % confidence level using a two-sided *t*-test.

744

745